Journal of Chromatography A 1641 (2021) 461981

Contents lists available at ScienceDirect

Journal of Chromatography A

journal homepage: www.elsevier.com/locate/chroma

Analysis of complex particle mixtures by asymmetrical flow field-flow fractionation coupled to inductively coupled plasma time-of-flight mass spectrometry

Olga Meili-Borovinskaya[a,*], Florian Meier[b], Roland Drexel[b], Mohammed Baalousha[c], Luca Flamigni[a], Andreas Hegetschweiler[d], Tobias Kraus[d,e]

[a] TOFWERK AG, Thun, Switzerland
[b] Postnova Analytics GmbH, Landsberg, Germany
[c] Center for Environmental Nanoscience and Risk, Department of Environmental Health Sciences, Arnold School of Public Health, University of South Carolina, Columbia, South Carolina, United States
[d] INM - Leibniz Institute for New Materials, Saarbrücken, Germany
[e] Colloid and Interface Chemistry, Saarland University, Saarbrücken, Germany

ARTICLE INFO

Article history:
Received 3 August 2020
Revised 2 February 2021
Accepted 7 February 2021
Available online 9 February 2021

Keywords:
Asymmetrical flow field-flow fractionation
Inductively coupled plasma time-of-flight mass spectrometry
Nanoparticles
Multi-element particles
Complex samples

ABSTRACT

Asymmetrical flow field-flow fractionation (AF4) hyphenated with inductively coupled plasma-mass spectrometry (ICP-MS) has been widely used to characterize metal containing particles. This study demonstrates the advantages of coupling AF4 with ICP-time-of-flight mass spectrometry (ICP-TOFMS) in standard and single particle modes to determine size distribution, elemental composition, and number concentration of composite particles. The coupled system was used to characterize two complex particle mixtures. The first mixture consisted of particles extracted from micro-alloyed steels with two size populations of different elemental composition. The second mixture consisted of particles extracted from soil spiked with various engineered nanoparticles (ENPs). The equivalent hydrodynamic sizes of individual micro-alloyed steel particles were up to 6 times larger than the sizes determined by single particle (sp)-ICP-TOFMS. The larger AF4 sizes were attributed to the presence of a surface coating, which is not reflected in the core size determined by sp-ICP-TOFMS. Two particle populations could not be separated by AF4 due to their broad size distributions but were resolved by sp-ICP-TOFMS using their unique elemental signatures. Multi-angle light scattering and ICP-TOFMS signals of soil suspensions increased with the spiked ENP concentrations. However, only after conducting full element screening and single particle fingerprinting by ICP-TOFMS could this increase be attributed to enhanced extraction efficiency of natural particles and the risk for false conclusions be eliminated. In this study, we describe how AF4 coupled to ICP-TOFMS can be applied to study complex samples of inorganic particles which contain organic compounds.

1. Introduction

Asymmetrical flow field-flow fractionation (AF4) is a flow-based fractionation technique which separates particles according to their hydrodynamic sizes [1–3]. Coupled with common detectors such as ultraviolet-visible spectroscopy (UV–Vis), multi-angle light scattering (MALS), or dynamic light scattering (DLS), AF4 measures particle size and particle concentration [4–6]. For the analysis of metal-containing particles, AF4 is often used in combination with inductively coupled plasma-mass spectrometry (ICP-MS) which provides particle concentration detection limits (μg L^{-1}, ng L^{-1}) far below the detection limits of UV–Vis, MALS, or DLS [7,8]. ICP-MS also offers higher specificity, because it can measure individual metals in a particle population, and multi-element capabilities which enable studying, for example, the composition of natural particles [9] and the interactions of engineered nanoparticles (ENPs) with natural colloids [10–13].

Sequential ICP-MS mass analyzers, such as quadrupole and magnetic sector field, are commonly used for coupling with AF4. With these analyzers only a limited number of isotopes can be selected for measurement to avoid skewing/shifts of elemental size distributions due to sequential signal recording. The choice of isotopes requires prior knowledge on the elemental composition of all

* Corresponding author.
E-mail address: borovinskaya@tofwerk.com (O. Meili-Borovinskaya).

https://doi.org/10.1016/j.chroma.2021.461981
0021-9673/

particles in each sample in order not to miss key sample information. This information can be gained by prescreening all samples but is time consuming. In this study, we online-coupled a time-of-flight (TOF) mass spectrometer to AF4 for the first time. TOF offers several advantages compared to quadrupole and sector field systems due to its simultaneous detection capabilities. Using TOF, untargeted analysis is conducted by default, ensuring the detection of all particles in a given sample at once without the need for sample prescreening, and thereby minimizing information losses.

We used ICP-TOFMS in both conventional mode and single particle mode, also called single particle (sp)-ICP-MS. In conventional mode, particles are size separated in the AF4 channel, and the ICP-TOFMS, in addition to size distributions gained from the AF4 system itself, records the isotope signature of eluting particles, providing the bulk elemental composition of all particle populations.

In single particle mode [14], the AF4 separation is performed on a highly diluted particle sample (10^6–10^7 particles mL^{-1}), and the ICP-TOFMS measures all isotope signals of individual particles eluting from the AF4. These isotope signals are then converted to particle number concentrations and to element masses, which are used to estimate particle sizes [15,16]. The concept of online coupling of the AF4 with sp-ICP-MS and its advantages have been recently demonstrated by Huynh et al. using monodisperse core-shell particles [17] and Hetzer et al., who investigated the release of nanosilver from packaging films [18]. In multi-detector AF4-sp-ICP-MS, particle sizes can be measured by three independent methods in the same run: by sp-ICP-MS, by MALS or DLS, and by calibrating the retention times. The sp-ICP-MS measured size is mass-based and does not include the information about particle porosity, particle coating or particle true composition (e.g., organic moieties or non-metals which are not detectable by sp-ICP-MS). Such properties, however, can be attained from the retention times and in-line MALS or DLS measurements. sp-ICP-MS, on the other hand, directly measures particle number concentration. This helps to overcome the current limitation of conventional AF4-ICP-MS, where the particle number concentration is often estimated from the element mass concentration and the particle size using certain assumptions about particle composition, shape, and density that are strictly applicable only to monodisperse particles [19]. In addition, the AF4 channel physically removes ionic species that could potentially reduce the sp-ICP-MS particle size detection limit [17,20].

Online coupling of the AF4 with sp-ICP-MS involves certain challenges. In some cases, MALS and especially DLS detectors will be insensitive to the low particle number concentration required for sp-ICP-MS. An additional run at higher particle number concentration can be conducted in order to gain the missing size information, and fractions of eluting particles can be collected at given time intervals and measured with the standalone sp-ICP-MS after proper dilution (offline coupling) [21–25], or a split flow setup can be introduced in front of the ICP-MS inlet for online sample dilution. The analysis by online coupling is less labor intensive than by offline coupling but requires optimization of the injected particle number concentration to minimize/avoid particle coincidences in sp-ICP-MS during the entire elution time. This concentration matching is practically challenging and requires several runs at different dilutions to determine the optimal conditions for all eluting particles.

ICP-MS must be operated at µs- or ms-time resolutions in order to resolve individual particle events when used as a single particle detector. The scanning speed of sequential instruments is not high enough to register more than one isotope (in some cases 2 isotopes [26]) within the extremely short signal (few hundred microseconds) generated by a single particle [27]. Single particle detection using TOF technology [28] ensures the measurement of all isotopes in each individual particle, provided the concentration of these isotopes is above the detection limit, and has already demonstrated its value for the nanoparticle research in material science [28,29], as well as environmental, [10,30] and food science [31]. For instance, TOFMS was able to distinguish pure CeO_2 ENPs from Ce-containing natural nanoparticles (NNPs) based on elemental composition of individual particles and count particles from these two classes independently [10].

The aim of this study was to demonstrate the potential of online coupling of AF4 with ICP-TOFMS for the characterization of complex multi-element particles. For this purpose, we used particles with two size populations of different elemental composition extracted from micro-alloyed steel that have previously been characterized using sp-ICP-TOFMS and scanning transmission electron microscopy (STEM) [29]. In addition, we applied the hyphenated system to study samples containing environmental particles extracted from a soil which was spiked with various ENPs. We showed that by using both the AF4-sp-ICP-TOFMS and the conventional AF4-ICP-TOFMS in a complementary manner we could measure particle size distributions by three independent methods (calibrating retention times, MALS, and sp-ICP-MS), particle number concentration, and elemental composition of both the entire particle population and individual particles.

2. Material and methods

2.1. Ti and Nb carbonitride particles

The extraction of NbCN and TiNbCN particles from steel and sample preparation procedure have been described elsewhere [29]. The micro-alloyed steel sample used here contained small precipitates composed of TiC, TiN, NbC, and NbN. All four compounds have a face centered cubic crystal structure. They form complete solid solutions in which Nb and Ti are interchangeable and N and C are interchangeable. Therefore, the extracted particles are not stoichiometric as 1:1:1:1, but are rather represented as (Nb)(C,N) and (Nb,Ti)(C,N). However, since we could not measure the C and N content in individual particles due to high detection limits of both, we assumed the ratio of N and C to be 1:1 and used it for further size calculation. For simplicity, (Nb)(C,N) and (Nb,Ti)(C,N) are referred to in the text as niobium and titanium carbonitride particles or as NbCN and TiNbCN, respectively. The extracted particles were suspended in water containing traces of Fe at concentration $<5 \times 10^{-3}$ mmol and stabilized with Disperbyk-2012. The bulk concentrations of Nb and Ti were measured by ICP-OES (at Leibniz Institute for New Materials, Saarbrücken, Germany) to be 25 mg L^{-1} and 13 mg L^{-1}, respectively. The suspension was sonicated for 10 min in an ultrasonic bath at 160 W and used undiluted for the conventional AF4-ICP-TOFMS, diluted in ultrahigh purity (UHP) water 150 times for the AF4-sp-ICP-TOFMS, and diluted 10^5 times for the standalone sp-ICP-TOFMS.

2.2. Spiked soil samples

Stock suspensions of a mixture of TiO_2, CeO_2, and Fe_2O_3 (see Table 1) ENPs were prepared at concentrations of 0.05, 0.5, and 5 mg kg^{-1}. A soil sample was collected from the top 15 cm in the Chester County, South Carolina, USA in March 2017. The soil has a moderate fine granular structure and is friable, nonsticky and nonplastic. 1.5 g of the soil was well-mixed with 1.5 ml of ENP stock suspension and was left to dry for 48 h under the fume hood at room temperature. Nanoparticles were then extracted from the spiked soils following the optimized extraction protocol presented elsewhere [9,32]. Briefly, a 30 ml aliquot of sodium pyrophosphate was added to the dry soil-ENP mixture at the ratio of 1 g soil:20 ml solution and the pH was adjusted to 10 using NaOH. The mixtures were stirred for 24 h. The samples were then sonicated for 1 h and centrifuged to separate 100 nm (130 min,

Table 1
Characteristics of engineered nanoparticles used in spiking experiments.

NPs	Formula	Supplier	Particle size	Size from
Iron oxide	Fe_2O_3	Sigma Aldrich	< 50 nm	Brunauer, Emmett and Teller
Titanium dioxide-103	TiO_2	Joint Research Center-European commission	20–100 nm	Transmission electron microscopy
Cerium dioxide-212	CeO_2	Joint Research Center-European commission	135 nm	Collective light scattering

Table 2
Operating conditions of the AF4 and the icpTOF R.

AF4 parameters	Steel particles and soil extract with <100 nm	Soil extract with <450 nm	icpTOF R parameters	
Injection volume	20 µl	20 µl	Plasma power	1550 W
Cross flow	1.5 ml/min	1.3 ml/min	Nebulizer gas flow rate	1 l/min
Focus pump flow rate	1.8 ml/min	1.6 ml/min	Plasma gas flow rate	14 l/min
Delay time	2 min	2 min	Auxiliary gas flow rate	0.8 l/min
Injection time (including focusing)	5 min	5 min	Flow rate of a gas mixture (7% H_2 in He) in the collision/reaction cell	3 ml/min
Transition time	0.5 min	0.5 min	Integration time (single particle mode)	3 ms
Elution program	55 min, power, exponent 0.3	75 min, power, exponent 0.3	Integration time (conventional mode)	0.5 s
Channel flow rate	0.5 ml/min	0.5 ml/min		
Detector flow rate (through 60% smart stream splitting)	0.3 ml/min	0.3 ml/min		
MALS integration time	0.6 s	0.6 s		
Time to transfer the sample from MALS detector to the ICP	1 min	1 min		

4000 g) and 450 nm (30 min, 2000 g) fractions assuming particle density of 2.5 g cm $^{-3}$. This corresponds to a size cutoff of 50 nm and 221 nm for CeO_2 ENPs (density = 7.22 g cm $^{-3}$); 68 nm and 307 nm for TiO_2 ENPs (density = 4.23 g cm $^{-3}$); and 60 nm and 268 nm for Fe_2O_3 ENPs (density = 5.24 g cm $^{-3}$).

2.3. AF4-ICP-TOFMS and AF4-sp-ICP-TOFMS

A metal-free AF4 system (AF2000 MF, Postnova Analytics GmbH, Germany) equipped with a smart stream splitter (Postnova PN1650), ICP-MS module (Postnova PN9050), UV–Vis detector (Postnova PN3211 UV), and a MALS detector (Postnova PN3621 MALS) was coupled to the ICP-TOF mass spectrometer (icpTOF R, Tofwerk, Switzerland) for all experiments. A comprehensive description of the icpTOF R instrument and its capabilities for single particle detection can be found in Hendriks et al. [33]. Operating conditions of the AF4 and icpTOF R are listed in Table 2. The AF4 channel was equipped with a 350 µm Mylar spacer and a 10 kDa regenerated cellulose membrane placed onto a ceramic frit (Postnova Analytics GmbH, Germany). The carrier phase for the analysis of Ti and Nb carbonitride particles was 0.005 wt% SDS (SigmaAldrich, USA) and 0.4 mg L^{-1} NaOH (SigmaAldrich, USA) in UHP water. For the soil extracts, the carrier phase was composed of 0.003 wt% NaN_3 (SigmaAldrich, USA), 0.01 wt% Novachem (Postnova Analytics GmbH, Germany), and 1 mM $NaNO_3$ (SigmaAldrich, USA) in UHP water. The start of the ICP-TOFMS acquisition was synchronized with the start of the AF4 run using a 5 V TTL trigger signal. For the conventional analysis, the undiluted samples were used. For the sp-ICP-TOFMS, the injected particle concentration was optimized to achieve the optimal particle rate at the detector (< 20 particles/s) across the entire elution peak, meaning the probability of detecting two particles in one integration time was below 0.2%. The AF4 channel was rinsed for 1 min after each run and the UHP water was measured at the beginning and at the end of each sample type to check for memory effects. MALS geometric diameter (D_{geo}) was calculated from the radius of gyration (R_g) applying the hard sphere model using the following correlation: $D_{geo} = 2 \times R_g / \sqrt{(3/5)}$. The shape factor was defined as R_g / R_h, where R_h is the equivalent hydrodynamic radius calculated from retention times. Retention times were calibrated with polystyrene nanobeads (ThermoFisher Scientific, USA) with a mean diameter (hydrodynamic diameter certified by DLS) of 20, 41, 81, and 152 nm diluted in UHP water. The concentration of nanobeads was 20 mg kg^{-1} for 20 nm and 41 nm and 200 mg kg^{-1} for 81 nm and 152 nm, respectively. Nanobeads were measured at the beginning and at the end of each sequence to control the system reproducibility. The second-degree polynomial function was used to fit the calibration curves. Examples of calibration curves are shown in Figure S1. Low and high detection limits for the equivalent hydrodynamic diameter are accurately defined by minimum and maximum sizes of the calibration beads, which were 20 nm and 152 nm, respectively. It should be noted that the particle sizes >152 nm were calculated by extrapolation of the calibration curve and are, therefore, less accurate. By calibrating the AF4 with a nanobead mixture of a broader size range (20, 41, 81, 152, and 350 nm) in a separate run (after the experiments) and comparing the accuracy of size calculation for retention times <43 min, we concluded that sizes calculated with the calibration range of 20–152 nm do not deviate by more than 14% from sizes calculated with the calibration range of 20–350 nm.

2.4. Particle quantification with sp-ICP-TOFMS

For the steel extract particles, the elemental mass in individual particles and the particle number concentration were determined using the method reported by Pace et al. [16]. Element-specific instrument sensitivities were measured with a mixture of Ti single element standard and Nb single element standard (Inorganic Ventures, USA) in the concentration range of 0.05–100 µg kg^{-1}. Au nanoparticles (AuNPs) with a certified particle mean diameter of 60 nm (RM 8013, NIST, USA) and Au element standard solutions (InorganicVentures, USA) prepared in UHP water were measured to determine the transport efficiency of the sample introduction system. The transport efficiency was calculated using the method described by Pace et al. [16]. The measurement of calibration solutions and AuNP was conducted offline by decoupling the AF4 from the sample introduction system of the ICP-TOFMS. The sample uptake flow rate in offline mode was identical to the output flow of the AF4 system. To determine the detection limits for Ce and La in the spiked soil samples, element-specific sensitivities were mea-

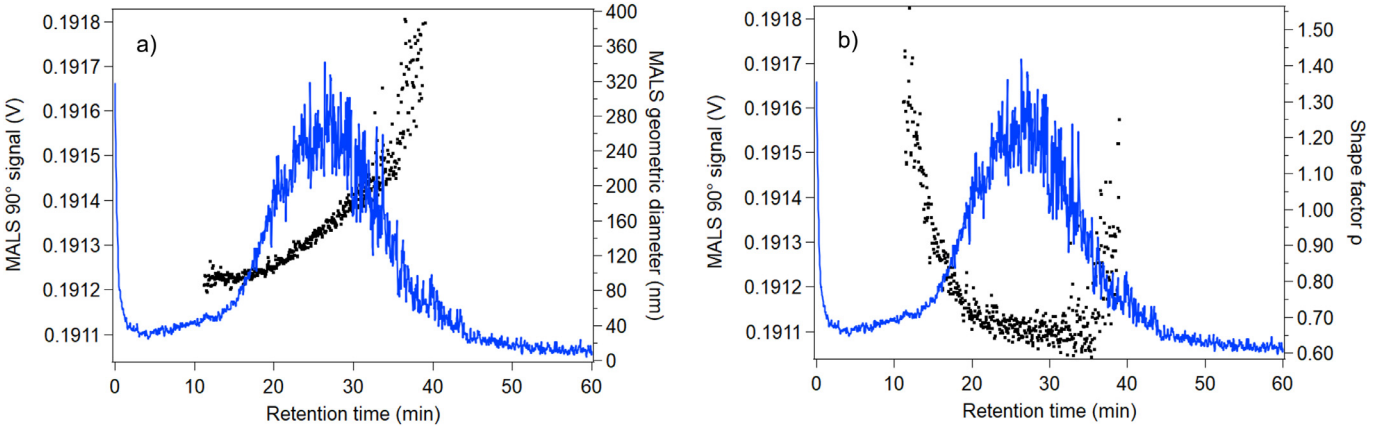

Fig. 1. a) MALS 90° signals of NbCN and TiNbCN particles with MALS geometric diameter shown on the plot as black dots. b) MALS 90° signals of NbCN and TiNbCN particles with the shape factor shown on the plot as black dots.

sured with a rare earth element standard solution (Ce, Dy, Er, Eu, Gd, Ho, La, Lu, Nd, Pr, *Sc*, Sm, Tb, Th, Tm, U, Y, Yb) of 10 µg kg^{-1} (Inorganic Ventures, USA). The transport efficiency was determined in the same way as for NbCN and NbTiCN particles.

2.5. sp-ICP-TOFMS data processing

Particle signal processing was realized using the particle processing module in TofPilot software (Tofwerk, Switzerland). Particle/noise signal separation was performed using a running window of 100 data points. For each window, a threshold was calculated according to Eq. (1), which describes low intensity noise more accurately than the 3*sigma approach [34]:

$$\text{Threshold} = \text{mean} + (3.29 \times \text{SD} + 2.71) \quad (1)$$

where mean and standard deviation (SD) of signals are calculated in counts for each window of 100 data points.

All peaks exceeding the threshold were selected as particle signals and extracted from the data set. This process was repeated iteratively until no more peaks were detected. The signal of dissolved ions (mean of all signals left after thresholding in the interval of 100 points, which includes truly dissolved ions and NPs below the size detection limit) was subtracted from each particle signal. At the TOFMS integration time of 3 ms, a small fraction of particle signals was split between two integration times. These split-signals were summed up after peak/background subtraction. The time dimension of each isotope signal in each particle was preserved throughout the data processing, allowing to look for element correlations in individual particles and to calculate particle retention times. For standard AuNPs, the median signal intensity was used as an approximation for the statistical mode. Counts per particle were converted to mass per particle for each element. Masses of NbCN and TiNbCN particles were calculated summing up the mass of Ti and Nb and applying a mass correction factor to compensate for the C and N contribution, which cannot be measured by sp-ICP-MS technique due to very high detection limits. Masses were converted to volumes using a density of 7.8 g cm^{-3} for NbCN and of 6.6 g cm^{-3} for TiNbCN, respectively. Sizes were calculated assuming the particles are spherical. Particle number concentrations were calculated from the total number of particle signals detected per run, corrected by transport efficiency and total sample volume measured, as described elsewhere [16].

Detection limits were calculated from the signals of UHP water using Eq. (2):

$$\text{LOD} = 3.29 \times \text{SD} + 2.71 \quad (2)$$

where SD is the standard deviation of the background signal in counts.

LODs in counts were converted to particle sizes in the same way as described above.

Particle number concentration recoveries in the AF4-sp-ICP-TOFMS analysis were calculated using Eq. (3):

$$\text{Recovery} = C_{\text{AF4-sp-ICP-TOFMS}}/C_{\text{sp-ICP-TOFMS}} \times 100\% \quad (3)$$

where $C_{\text{AF4-sp-ICP-TOFMS}}$ is the particle number concentration determined by AF4-sp-ICP-TOFMS and $C_{\text{sp-ICP-TOFMS}}$ is the particle number concentration determined by standalone sp-ICP-TOFMS.

3. Results and discussions

3.1. AF4-ICP-TOFMS of carbonitride nanoparticles

NbCN and TiNbCN particles extracted from micro-alloyed steel were used as a model to test the feasibility of the AF4-ICP-TOFMS in both conventional and single particle modes to determine particle size distributions and particle number concentrations of composite particles. STEM studies of Hegetschweiler et al. [29] on the same steel extracts indicated that NbCN and TiNbCN particles have a mean diameter of 28 nm and 86 nm, respectively, representing two different size populations with different elemental compositions. An AF4-MALS fractogram of an undiluted particle suspension is shown in Fig. 1. No separation of NbCN and TiNbCN particles could be achieved after testing various AF4 conditions suggesting broad particle size distributions of both particle types. The geometric diameters, calculated from the MALS radius of gyration, ranged from 70 to 300 nm across the peak (Fig. 1a) and were consistently smaller than the equivalent hydrodynamic diameters (Fig. 2). This observation can be explained by the presence of a low mass or low density shell around these particles that does not significantly contribute to the MALS signal but increases the hydrodynamic sizes of these particles and, thus, retention times. This is also reflected in the shape factor with the average value calculated over 50% of the MALS peak width of 0.67 indicating a spherical shape with a dense core surrounded by a less dense, presumably organic shell [35,36]. No UV–Vis signal was detected most likely due to low particle number concentration. Since the composition of these particles was well known, the ICP-TOFMS signals did not provide any additional information and are, therefore, not presented.

3.2. AF4-sp-ICP-TOFMS of carbonitride nanoparticles

For the single particle run, the sample was diluted 150 times prior to injection. Fig. 3 shows an overlay of MALS 90° signals and

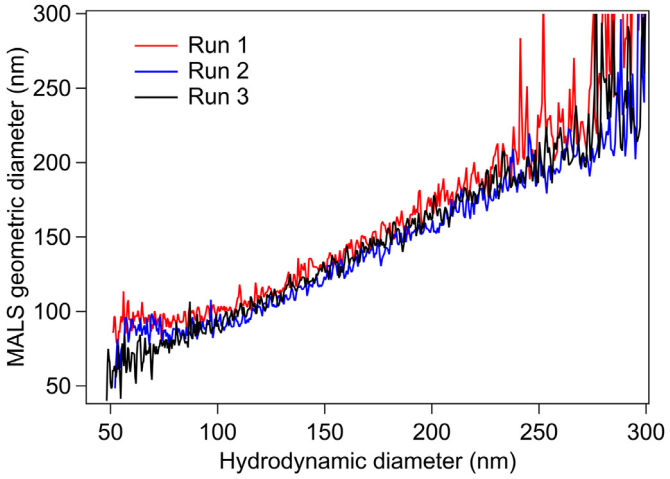

Fig. 2. MALS geometric diameters from three consequent runs plotted against the equivalent hydrodynamic diameters obtained from the AF4 retention times.

ICP-TOFMS signals of fractionated particles. As in the conventional run, the AF4-MALS signal is a single broad peak and does not allow discriminating the two particle populations. However, these two particle populations could be distinguished in the TOFMS based on their different elemental compositions. The first population consisted of smaller particles which contained Nb only (Fig. 3b); whereas the second population eluted later and contained both Ti and Nb (Fig. 3c). These results suggest that the first size population is NbCN particles and the second population is TiNbCN particles and is in good agreement with our prior knowledge on these particles. ICP-TOFMS single particle signals detected in the retention time interval of 11–38 min were converted to particle sizes and were compared to those measured by the standalone sp-ICP-TOFMS (Fig. 4). For both particle types, the size distributions measured with and without AF4 were almost identical, indicating no significant agglomeration of particles induced by the fractionation process in the AF4 channel.

Fig. 5 shows the mass-based diameters from sp-ICP-TOFMS plotted against the equivalent hydrodynamic diameters calculated in the time interval of 11–38 min. The geometric diameter could not be reliably calculated in this run due to low MALS signal intensity. The equivalent hydrodynamic diameter appears to be larger than the mass-based diameter for both particle populations with the mass-based diameter increasing less drastically across the retention time. The equivalent hydrodynamic size distribution is also much broader than the mass-based size distribution. This may be attributed to a combination of several factors including (i) the presence of particle agglomerates in the sample, (ii) the differences in the measurands obtained by AF4 and sp-ICP-TOFMS, (iii) deviations from the spherical shape assumed for the size calculation in both methods, (iv) the existence of an organic shell on the par-

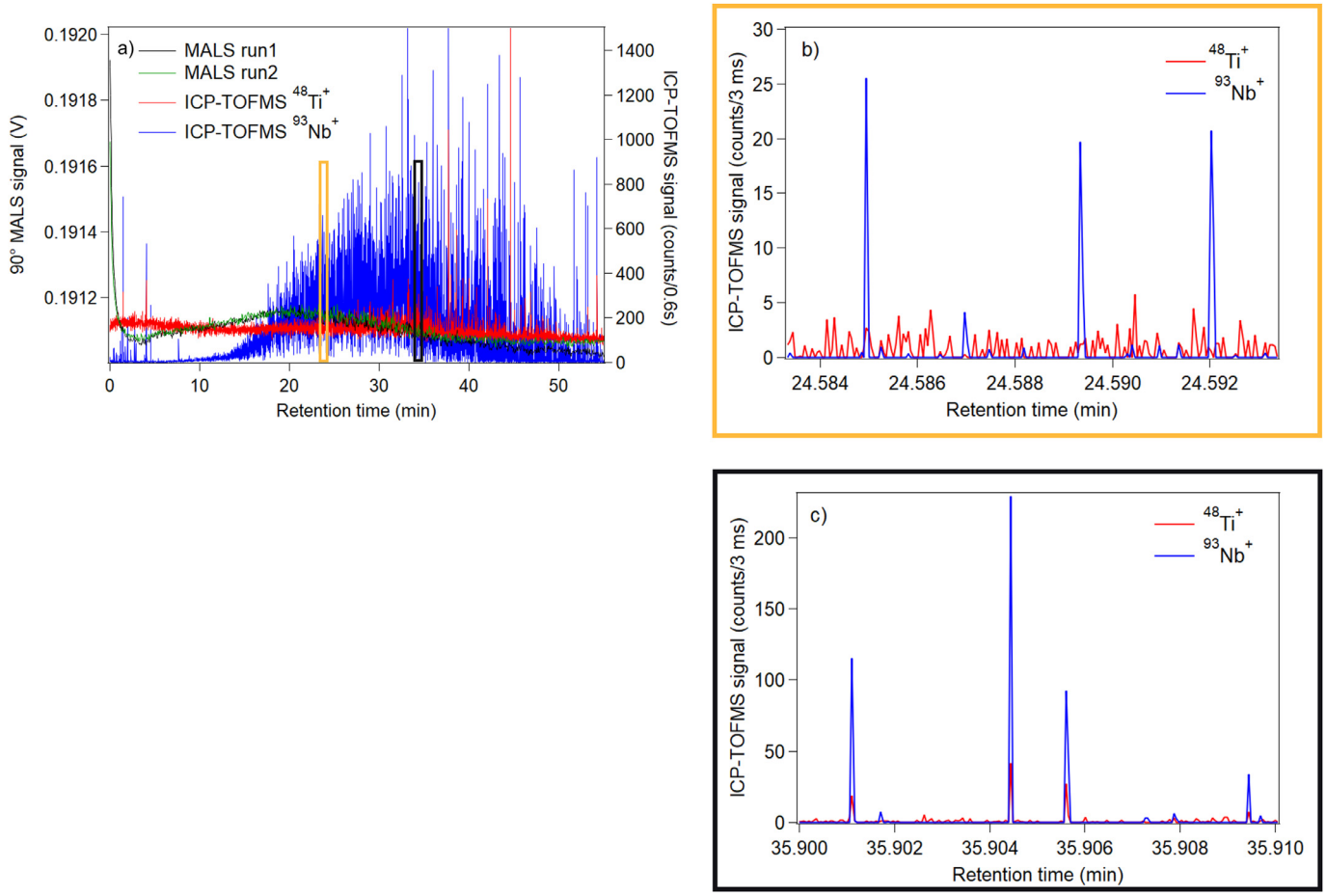

Fig. 3. a) MALS and ICP-TOFMS signals plotted against retention times. MALS signals from two replicates are shown. ICP-TOFMS signals were acquired with 3 ms integration time, but in this plot, data is binned over 0.6 s for a clearer data representation. b) ICP-TOFMS signal at the retention time of 24 min acquired with 3 ms integration time, showing particles containing Nb only, with Ti signal being the background noise only. c) ICP-TOFMS signal at the retention time of 35 min acquired with 3 ms integration time, showing particles containing both Nb and Ti. (For interpretation of the references to colour in this figure legend, the reader is referred to the web version of this article.)

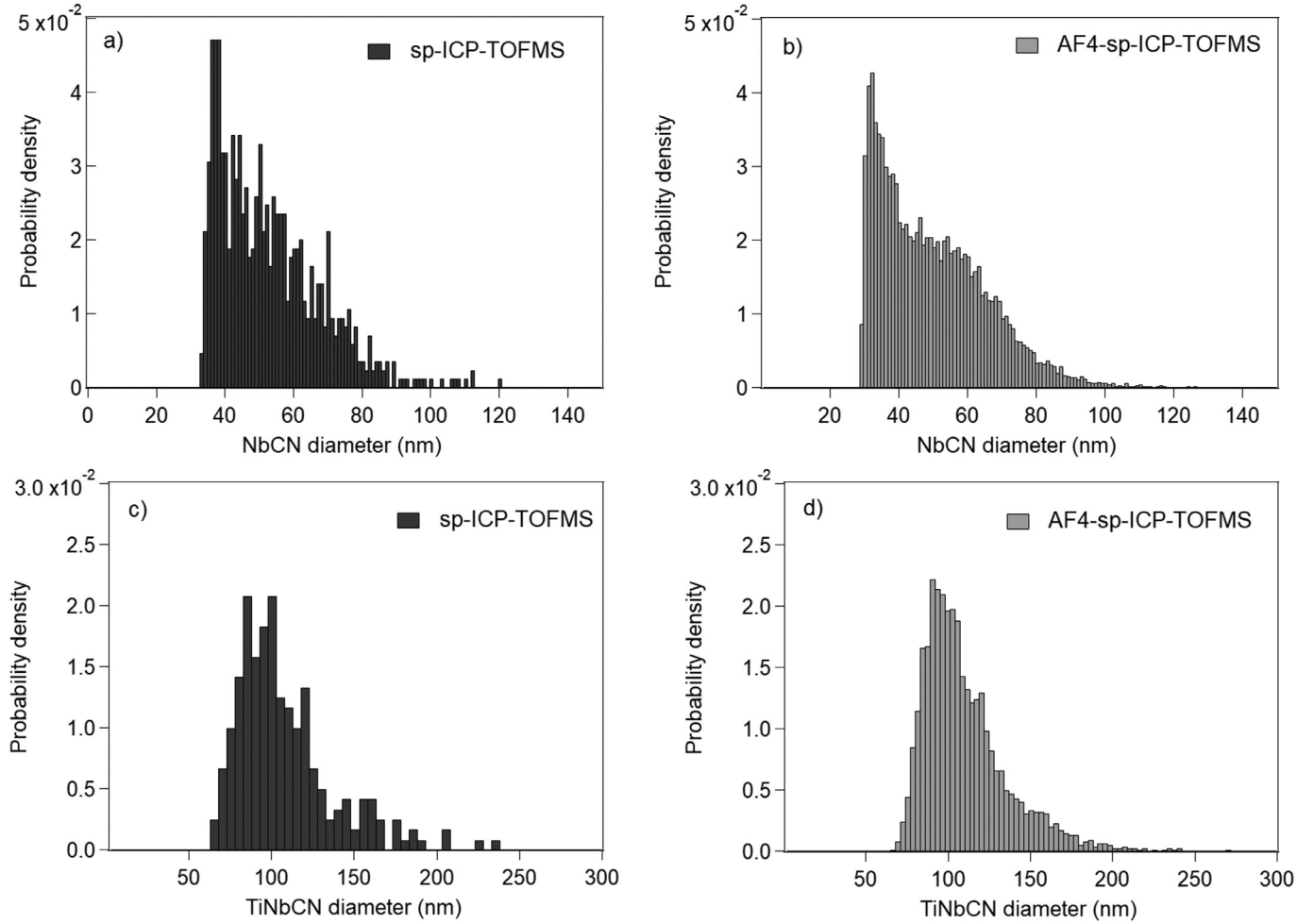

Fig. 4. Comparison of size distributions of NbCN and TiNbCN particles measured with the standalone sp-ICP-TOFMS (a,c) and the AF4-sp-ICP-TOFMS (b,d). The sizes were calculated from element masses measured in the sp-ICP-TOFMS. Larger number of particles was detected in a 60 min AF4-sp-ICP-TOFMS run than in a 1 min standalone sp-ICP-TOMS run. The histograms were normalized to probability density for an easier data comparison.

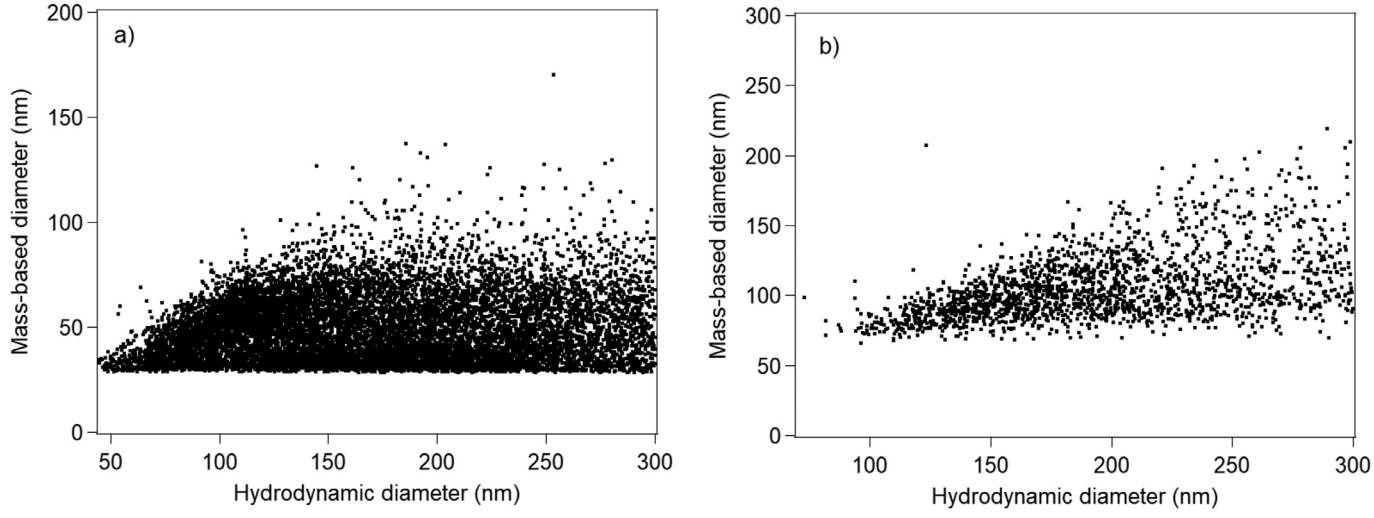

Fig. 5. Mass-based diameter of NbCN (a) and TiNbCN (b) particles obtained by sp-ICP-TOFMS plotted against the equivalent hydrodynamic diameter obtained from the AF4 retention times using polystyrene nanobeads as size standards.

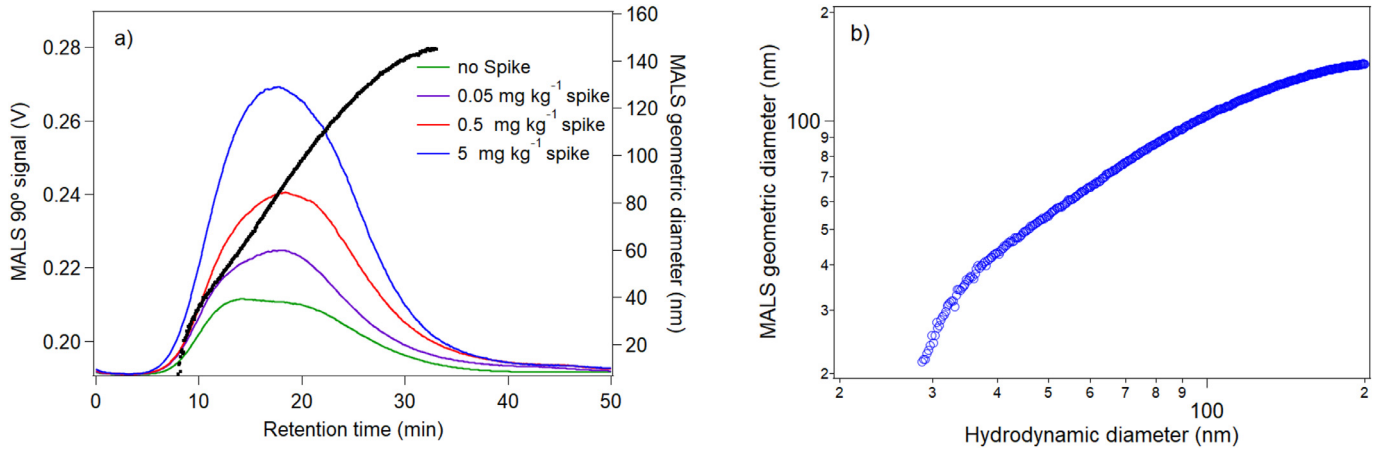

Fig. 6. a) MALS 90° signals of particles extracted from soil samples, spiked with the ENPs stock suspension of different concentrations. The MALS geometric diameter for 5 mg kg^{-1} spiked sample is shown on the plot as a black line. b) MALS geometric diameter vs equivalent hydrodynamic diameter of 5 mg kg^{-1} spiked sample. In the range of 40–100 nm, both methods gave similar sizes with the MALS sizes being smaller at the leading and tailing side of the fractogram.

ticles, and (v) particle-specific interactions with the membrane in the AF4 channel.

If particles form agglomerates, the equivalent hydrodynamic diameter will be larger than the mass-based size and its size range broader. This is because the size obtained from sp-ICP-TOFMS is calculated by summing masses of all primary particles within the agglomerates. The size calculated from the mass will always be smaller than the size of the agglomerate with its less compact, fractal geometry. STEM analysis indicated that primary NbCN and TiNbCN particles are close to spherical [29], and, therefore, particle sphericity is a valid assumption for size calculations.

Agglomeration explains the broadening of the hydrodynamic particle size above mass-based sizes, but it does not explain why even the primary particles appear larger. Organic shell on the inorganic particle core that is not detected by sp-ICP-TOFMS or MALS is the most probable explanation for the overall increase of the hydrodynamic diameter. The particles were extracted from steel using the Disperbyk-2012 surfactant that is based on a surface-active polymer which covers the particle surface. The observed combination of larger average hydrodynamic particle sizes and wider hydrodynamic size distributions suggest the presence of both agglomerates and organic coatings. This additional size information gained by AF4 is crucial for an accurate data interpretation of the sp-ICP-TOFMS results.

The particle number concentration determimed byAF4-sp-ICP-TOFMS was lower than that from standalone sp-ICP-TOFMS. If the concentration measured with the standalone sp-ICP-TOFMS is taken as a reference, the concentration recoveries obtained with the AF4-sp-ICP-TOFMS were 78% for NbCN and 47% for TiNbCN. Particle losses in the AF4 system is one possible explanation for this incomplete recovery. The lower recovery of TiNbCN particles compared to NbCN particles could partially be attributed to their larger size, which is likely to result in higher membrane particle interaction as larger particles are moving closer to the channel membrane during the fractionation process.

In order to test this hypothesis, we measured UHP water blank after the particle sample. The results did not indicate substantial memory effects. The lower recovery of TiNbCN particles (47%) compared to NbCN particles (78%) is most likely explained by their higher size detection limits in the AF4-sp-ICP-TOFMS compared to the standalone sp-ICP-TOFMS. The size detection limits in the sample, estimated from the background signal left after running the particle signal removal algorithm, were 28 nm for NbCN and 48 nm for TiNbCN particles in the standalone sp-ICP-TOFMS analysis, and 28 nm for NbCN and 62 nm for TiNbCN particles in the AF4-sp-ICP-TOFMS analysis. The higher LOD of TiNbCN particles, which explains poorer recovery of these particles, are due to higher Ti background signal most likely coming from solvent impurities. The run to run particle number concentration reproducibility (from 3 runs) from the AF4-sp-ICP-TOFMS analysis was 13% for NbCN and 7% for TiNbCN particles.

3.3. AF4-ICP-TOFMS of spiked soil samples

Extracts of the spiked soil samples were first measured with the AF4-ICP-TOFMS in conventional mode without any sample dilution. Fig. 6a shows MALS signals of soil samples spiked with different concentrations of ENPs. The MALS signal intensity increased from unspiked to 5 mg kg^{-1} spiked sample. Particle geometric sizes were in the range of 20–140 nm and increased with the retention time, indicating good sample fractionation in AF4. The geometric diameter distribution and the equivalent hydrodynamic distribution obtained from retention times (Fig. 6b) were comparable in the range of 40–100 nm with MALS sizes being smaller at the leading and tailing part of the fractogram.

Ti, Fe and Ce ICP-TOFMS signals and UV–Vis signals also increased with the increase in the spiked ENP concentration (Fig. 7). The increase in the concentration of spiked elements can arise from both (i) the increased concentration of TiO_2, Fe_2O_3 and CeO_2 spiked engineered particles, and (ii) the increased extraction efficiency of natural particles containing these elements due to the introduction of residual surfactants (left after synthesis) together with ENP spikes, enhancing extraction efficiency of all particles. The ICP-TOFMS signals of Ti, Fe and Ce were integrated in the interval of 11 to 38 min for each elution peak and ratios of net signals (the signal of the unspiked sample was defined as a background and was subtracted from the sample signals) were calculated and are presented in Table 3. We observed an approximately twofold increase in element concentrations of Ti, Fe, and Ce in contrast to the expected tenfold increase. This shows that the extraction efficiency of ENPs was not proportional to the spiked concentration. This could be due to concentration-dependent particle agglomeration [37,38].

Along with Ti, Fe, and Ce, the following elements were detected: Mg, Al, Si, V, Mn, Co, Zn, Ga, As, Y, Zr, Nb, I, Cs, Ba, Pb, Th, U, La, and other rare earths elements (REE) such as Pr and Nd. The ICP-TOFMS signals of selected isotopes from the unspiked sample are shown in Fig. 8. This complex element mix

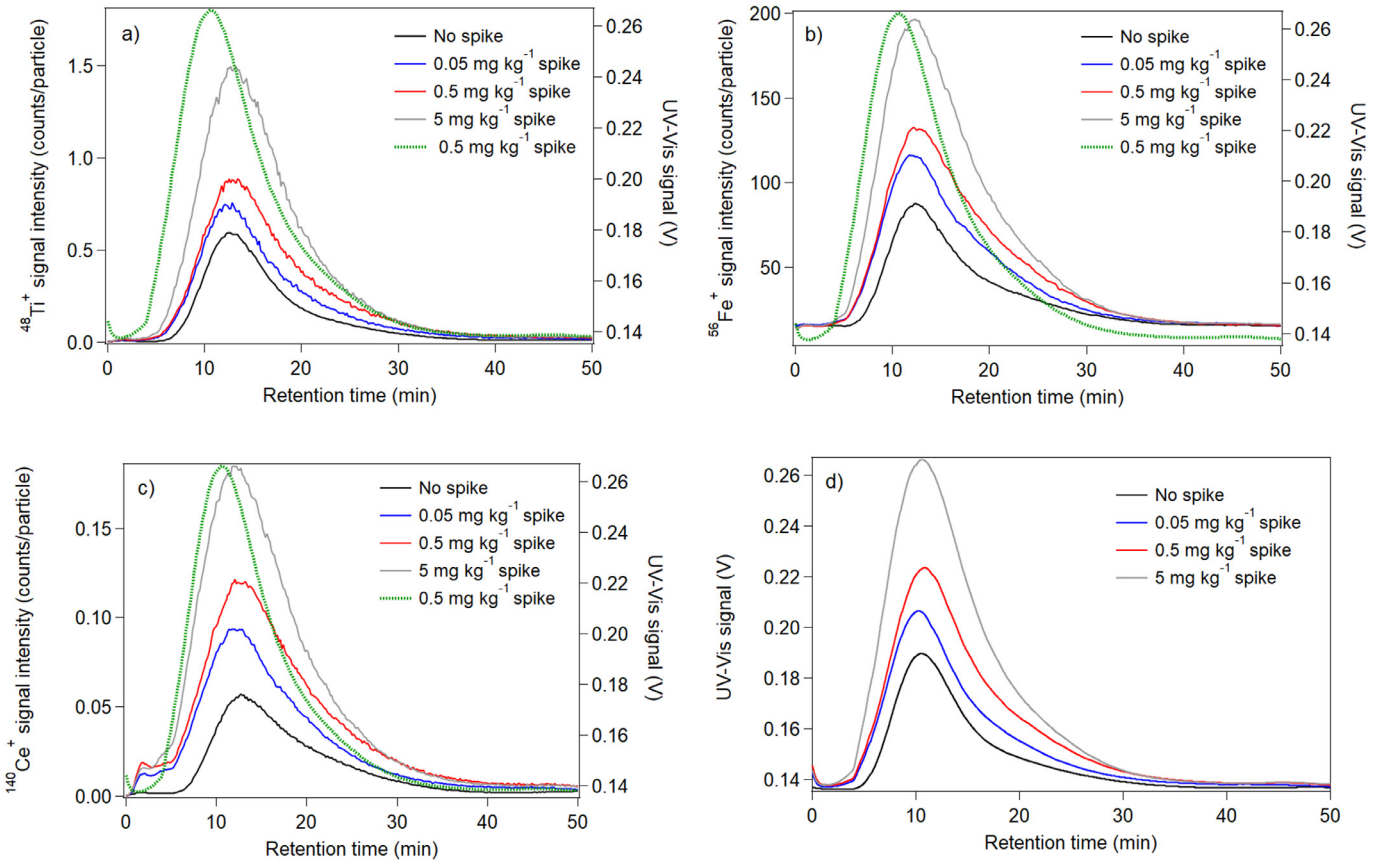

Fig. 7. ICP-TOFMS signals of a) Ti, b) Fe, c) Ce and d) UV–Vis signals of eluting particles from soil samples spiked with ENP suspensions of different concentrations.

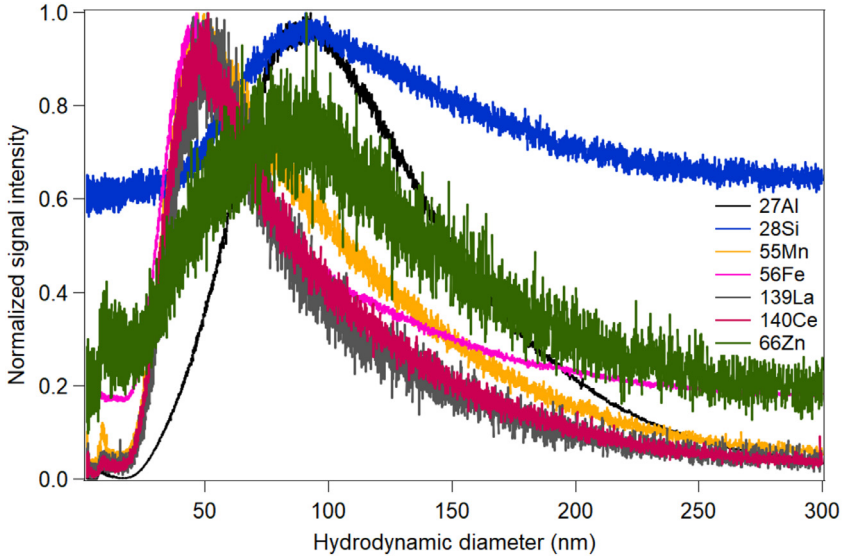

Fig. 8. Normalized ICP-TOFMS signals of eluting particles from the unspiked sample plotted against equivalent hydrodynamic diameter.

Table 3
Expected and measured Ti, Fe, and Ce concentration ratios in soil extract samples spiked with the ENPs at different concentrations.

Expected concentration ratio	Ti measured concentration ratio	Fe measured concentration ratio	Ce measured concentration ratio
0.5/0.05 = 10	2.0	1.6	1.7
5/0.5 = 10	2.3	2.0	2.0

Table 4
Ce/La ICP-TOFMS signal ratios from the soil extract samples spiked with the ENPs stock suspension of different concentrations.

Spike conc. (mg kg^{-1})	Ce/La
non	3.2
0.05	3.4
0.5	3.6
5	3.3

represents the soil composition and was common to all samples. The data suggest that there are three different populations of particles of different elemental compositions. The first particle population with a modal peak at ca. 13 min contained most of the detected elements, including Ti, Fe, and Ce. The second particle population with a modal peak at ca. 18 min contained mainly Zn. The third particle population with a modal peak at ca. 20.5 min contained Al and Si. It was hypothesized that the concentration of elements originating from natural particles remains constant with the increased spiked ENP concentrations, because the soil mass was identical for all spiked samples. However, their concentrations increased in the same way as the concentration of elements from the spiked ENPs (Table S1). This observation indicates that the twofold concentration increases of Ti, Fe, and Ce were not only due to the increased spiked ENP concentration, but also originated from the increase of the natural particle concentration due to a general increase in extraction efficiency. Therefore, conventional AF4-ICP-TOFMS was not able to distinguish the spiked ENPs from the strong background of natural particles containing Ti, Fe, and Ce. This example, however, demonstrates the advantage of detecting all elements in underpinning data interpretation.

Praetorius et al. described in their recent work [10] how the association of Ce primarily with La and other REEs in individual particles can be used to distinguish between pure-Ce engineered particles and non-pure natural Ce-containing particles. The authors proposed a fingerprint method which can recover concentrations of engineered CeO_2 at orders of magnitude lower than the concentrations of Ce-containing natural particles in soil samples that would be impossible to do with conventional ICP-MS. In our spiked samples, we observed a slight increase in Ce/La bulk mass ratios with the increase in spike concentration, except for the 5 mg kg^{-1} spiked sample, which showed a decrease (see Table 4). Each sample was run only once, hence, no ratio errors can be reported. The absence of a significant shift in the Ce/La ratio was again attributed to the much higher cerium concentration in the natural soil relative to the spiked CeO_2 concentrations.

3.4. AF4-sp-ICP-TOFMS of spiked soil samples

Two extracted soil suspensions with the highest and the lowest Ce/La bulk ratios (3.2 and 3.6 at 0 mg kg^{-1} spike and 0.5 mg kg^{-1} spike, respectively) were diluted 100 times and run in AF4-sp-ICP-TOFMS. Only few particles containing Ce (2 Ce and La and 37 Ce-only particles in the unspiked sample and 12 Ce and La and 89 Ce-only particles in the spiked sample) were detected. The majority of Ce-containing NPs had a hydrodynamic diameter < 150 nm with a modal peak at approximately 50 nm (Fig. 8), which would correspond to an even smaller particle core size. The size detection limit of pure CeO_2 particles, estimated from the signal of the UHP water blank, was 20 nm. The background signal intensity during the sample run was identical to the signal of the water blank and the same detection limit of 20 nm is applicable for the sample. To verify whether individual Ce-particles can be detected at all in these samples, the samples were diluted 10^5 and 10^6 times and measured with the standalone sp-ICP-TOFMS. Very few Ce-containing particles of relatively low intensity (corresponding to particle sizes close to detection limits) could be detected in the diluted samples. These results indicate that Ce-containing particles, both spiked and natural, present in the extracted soil suspensions were too small to be detectable in single particle mode. Fig. 8, however, suggests that Ce-containing particles with sizes up to 150 nm are present in these samples. The fact that we cannot detect any Ce from these particles is an indication that these particles have only a small amount of Ce, which is undetectable on a single particle level.

Samples spiked with 0.05 mg kg^{-1} and 0.5 mg kg^{-1} ENPs were centrifuged at a lower rpm to obtain a particle suspension with a larger size cut-off of 450 nm, diluted 100 times, and measured by AF4-sp-ICP-TOFMS. Ce was detected in particles either alone or associated with La, no other REE reported by Praetorius et al. [10] were detectable on a single particle level. Signals from the conventional AF4-ICP-TOFMS run of the unspiked sample filtered with 100 nm cut-off (Figure S2) demonstrate that beside La, Ce was also associated with other REE in natural particles. The ratio of REE signals to Ce signal is, however, much lower than the La/Ce ratio and explains why no REE could be detected in individual particles. Particle signals with Ce-only or with both Ce and La (CeLa) were separated in two populations and the $^{140}Ce^{+}$signal from both populations is shown in Fig. 9 together with the MALS signal. The $^{140}Ce^{+}$ signal from Ce-only particles was relatively low (most signals < 10 ions per particle) in comparison to $^{140}Ce^{+}$ signal in CeLa-containing particles. Higher signal intensity means higher mass content of Ce in CeLa particles and indirectly larger mean size. CeLa particles also eluted later in AF4 (Fig. 9), confirming their larger size. A Ce/La mean signal ratio of 1.3 ± 0.6 in individual particles was the same for both spike concentrations.

The fact that we did not detect any La in Ce-only particles does not necessarily imply that La is not present in these particles. The La mass in these particles may be below the detection limit of the sp-ICP-TOFMS, a very likely explanation because we expect comparable detection limits for Ce and La (CeO_2 – 20 nm, La – 22 nm) and the ratio of Ce/La of 3 according to the results of the bulk measurements. The number of both types of particles and their ratios were calculated from the entire run and are shown in Table 5. Excluding the possibility of concentration-dependent particle losses during sample preparation, we would expect to detect more of Ce-only particles in the 0.5 mg kg^{-1} spiked sample than in the 0.05 mg kg^{-1} one. The difference in Ce/CeLa particle number between two spike concentrations was, however, very minor. The results of this experiment support the hypothesis that most of detected Ce and CeLa particles are of natural origin and the recovered spike concentration was too low to be distinguishable from the natural background. The low recoveries of the spiked CeO_2 particles may be due to particle hetero-aggregation with soil organic matter leading to losses of the spiked particles during particle extraction and filtration [39].

Table 5
Number of Ce-only and CeLa particles and their ratios in the soil extract samples spiked with the ENP suspension of 0.05 mg kg^{-1} and 0.5 mg kg^{-1}.

Spike conc. (mg kg^{-1})	# of Ce-only particles	# of CeLa particles	# Ce/# CeLa
0.05	1230	1835	0.67
0.5	1494	2204	0.68

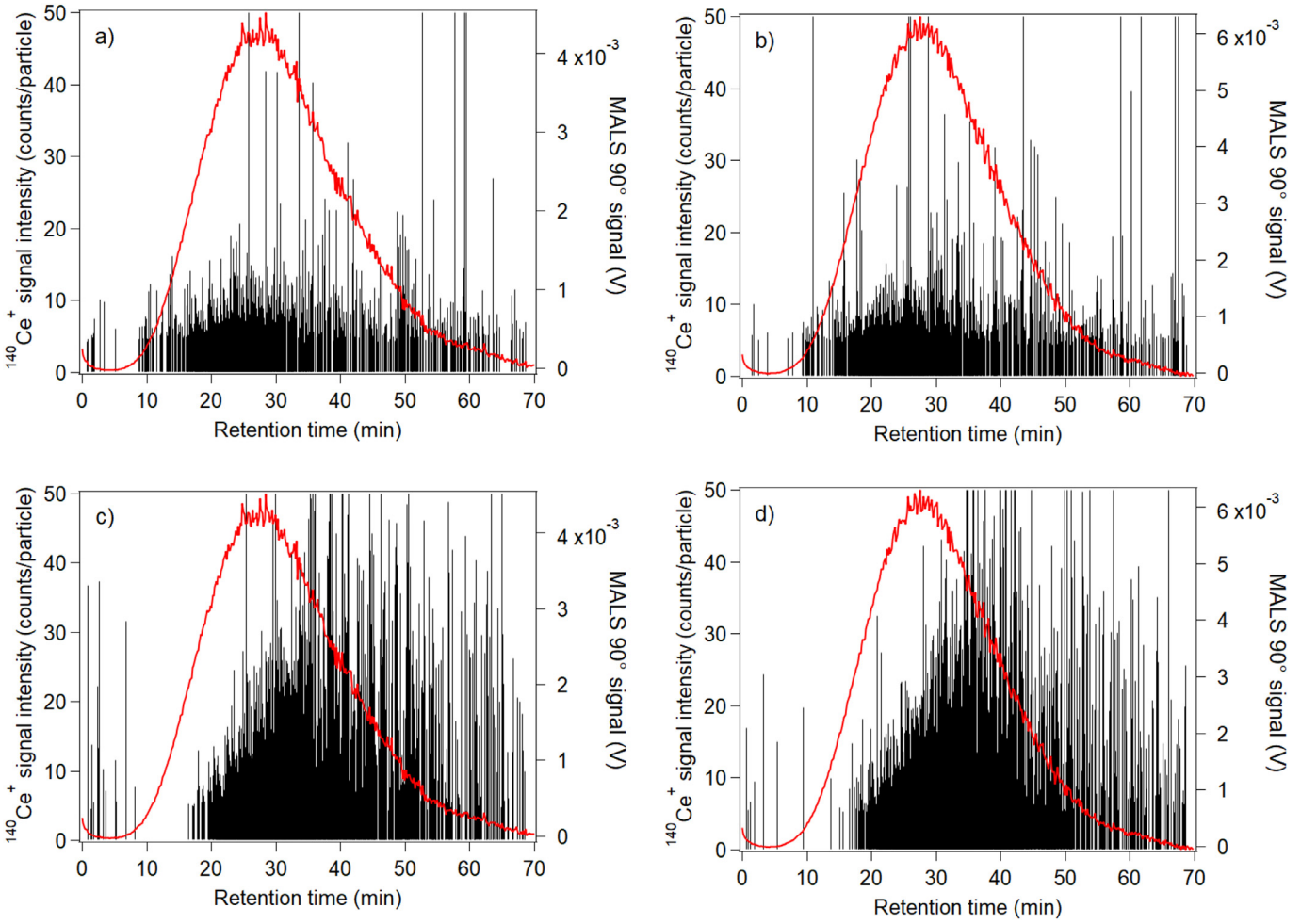

Fig. 9. MALS signals and $^{140}Ce^+$ signals of single Ce-only and CeLa-containing particles from soil extract samples spiked with the ENP stock suspension of different concentrations. a) Ce-only particles from 0.05 mg kg^{-1}spike. b) Ce-only particles from 0.5 mg kg^{-1}spike. c) CeLa particles from 0.05 mg kg^{-1}spike. d) CeLa particles from 0.5 mg kg^{-1}spike.

4. Conclusion

In this study, we demonstrated the advantages of online coupling of an AF4 with a simultaneous multi-element ICP-TOF mass spectrometer and using the hyphenated system in both conventional and single particle analysis modes. In conventional mode, TOFMS provides not only the concentration of target elements, but also the complete elemental composition of all particle populations. In single particle mode, in addition to mass-based metal core particle size from sp-ICP-MS, the equivalent hydrodynamic diameter from external size calibration and radius of gyration or geometric diameter from the MALS detector can be determined, providing additional information about the presence of agglomerates, organic moieties or coating. The sizes determined by AF4 are, therefore, closer to the true particle sizes than the core size from sp-ICP-MS, which is calculated from the element masses assuming an ideal particle geometry and a known density. The combination with TOFMS enables to study not only single element particles, as it is the case with sequential analyzers, but also complex particles that contain multiple elements. Furthermore, sp-ICP-TOFMS directly measures the particle number concentration of all particles in the same run that complements the concentration information determined in bulk.

For steel extract particles, we concluded that some particles are present in the form of agglomerates and most likely have an organic shell on their surface. This information would not be accessible with the standalone sp-ICP-TOFMS. The particle size distributions of NbCN (average diameter of 28 nm) and TiNbCN (86 nm) were relatively broad and could not be discerned by MALS detector following AF4 fractionation. These two types of particles, however, could be discriminated by sp-ICP-TOFMS analysis by tracing the unique elemental composition of individual particles.

We used particle suspensions extracted from soil samples that we spiked with a mixture of ENPs at different concentrations in order to demonstrate how combining different experiments with the AF4-ICP-TOFMS helps to study a complex particle sample. In conventional mode, we observed an increase of ICP-TOFMS signals of spiked elements with the increase of the spike concentration which could falsely be interpreted as the increase due to the spiked ENPs. Screening all elements in the extracted sample indicated that this increase is mostly due to the increase in the overall extraction efficiency of natural particles. Applying bulk element ratio measurements and single particle fingerprinting did not help to find the added particles in natural soils. We conclude that the spike concentrations of ENPs recovered from the soil were too low to be traceable in the presence of a high background of natural particles.

Our results and observations illustrate the valuable complementary information obtained by AF4-ICP-TOFMS and AF4-sp-ICP-TOFMS. The online coupling of AF4 with sp-ICP-TOFMS is, however, associated with several challenges. Finding an optimal particle number concentration for both AF4 and sp-ICP-TOFMS can be

difficult and not always possible due to sample complexity. The particle number concentration optimal for the sp-ICP-MS analysis is not always high enough for the MALS detector, as it was the case for NbCN and NbTiCN particles, and an additional run at higher particle number concentration was required to gain this missing information. Thus, we believe that for most of the samples both AF4-ICP-TOFMS and AF4-sp-ICP-TOFMS analyses must be conducted to gain the most detailed information about the sample. For some studies, offline coupling, which was beyond the scope of this work, might be more feasible than the online coupling and the suitability of the method must be evaluated on a case-by-case basis.

Declaration of Competing Interest

The authors declare that they have no known competing financial interests or personal relationships that could have appeared to influence the work reported in this paper.

CRediT authorship contribution statement

Olga Meili-Borovinskaya: Conceptualization, Methodology, Investigation, Data curation, Writing – original draft, Writing – review & editing, Visualization, Project administration, Funding acquisition. **Florian Meier:** Conceptualization, Methodology, Resources, Writing – review & editing, Funding acquisition. **Roland Drexel:** Data curation, Resources. **Mohammed Baalousha:** Methodology, Resources, Writing – review & editing, Funding acquisition. **Luca Flamigni:** Software. **Andreas Hegetschweiler:** Conceptualization, Resources, Writing – review & editing. **Tobias Kraus:** Conceptualization, Resources, Writing – review & editing.

Acknowledgements

This work has received funding from European Union Horizon 2020 Programme (H2020) under grant agreement n° 720952 (Project “ACEnano - Analytical and Characterization Excellence”) and from the Unites States National Science Foundation (grant number 1553909 and 1828055).

Supplementary materials

Supplementary material associated with this article can be found, in the online version, at doi:10.1016/j.chroma.2021.461981.

References

[1] J. Giddings, Field-flow fractionation: analysis of macromolecular, colloidal, and particulate materials, Science 260 (1993) 1456–1465.
[2] K.G. Wahlund, J.C. Giddings, Properties of an asymmetrical flow field-flow fractionation channel having one permeable wall, Anal. Chem. 59 (1987) 1332–1339.
[3] Y.U. Hachenberger, D. Rosenkranz, F.L. Kriegel, B. Krause, R. Matschaß, P. Reichardt, J. Tentschert, P. Laux, N. Jakubowski, U. Panne, A. Luch, Tackling Complex Analytical Tasks: an ISO/TS-Based Validation Approach for Hydrodynamic Chromatography Single Particle Inductively Coupled Plasma Mass Spectrometry, Materials (Basel) 13 (2020) 1447.
[4] V. Sogne, F. Meier, T. Klein, C. Contado, Investigation of zinc oxide particles in cosmetic products by means of centrifugal and asymmetrical flow field-flow fractionation, Journal of Chromatography A 1515 (2017) 196–208.
[5] T. Kowalkowski, M. Sugajski, B. Buszewski, Impact of ionic strength of carrier liquid on recovery in flow field-flow fractionation, Chroma 81 (2018) 1213–1218.
[6] D. Müller, M. Nogueira, S. Cattaneo, F. Meier, R. Drexel, C. Contado, A. Pagnoni, T. de Vries, D. Cohen, M. Portugal-Cohen, A. deMello, Integration of inverse supercritical fluid extraction and miniaturized asymmetrical flow field-flow fractionation for the rapid analysis of nanoparticles in sunscreens, Anal. Chem. 90 (2018) 3189–3195.
[7] T.K. Mudalige, H. Qu, S.W. Linder, Asymmetric flow-field flow fractionation hyphenated ICP-MS as an alternative to cloud point extraction for quantification of silver nanoparticles and silver speciation: application for nanoparticles with a protein corona, Anal. Chem. 87 (2015) 7395–7401.
[8] B. Meermann, K. Wichmann, F. Lauer, F. Vanhaecke, T.A. Ternes, Application of stable isotopes and AF4/ICP-SFMS for simultaneous tracing and quantification of iron oxide nanoparticles in a sediment–slurry matrix, J. Anal. At. Spectrom. 31 (2016) 890–901.
[9] Z. Yi, F. Loosli, J. Wang, D. Berti, M. Baalousha, How to distinguish natural versus engineered nanomaterials: insights from the analysis of TiO2 and CeO2 in soils, Environ Chem Lett 18 (2020) 215–227.
[10] A. Praetorius, A. Gundlach-Graham, E. Goldberg, W. Fabienke, J. Navratilova, A. Gondikas, R. Kaegi, D. Günther, T. Hofmann, F. von der Kammer, Single-particle multi-element fingerprinting (spMEF) using inductively-coupled plasma time-of-flight mass spectrometry (ICP-TOFMS) to identify engineered nanoparticles against the elevated natural background in soils, Environ. Sci.: Nano 4 (2017) 307–314.
[11] J. Makselon, N. Siebers, F. Meier, H. Vereecken, E. Klumpp, Role of rain intensity and soil colloids in the retention of surfactant-stabilized silver nanoparticles in soil, Environ. Pollution 238 (2018) 1027–1034.
[12] A.P. Gondikas, F.v.d. Kammer, R.B. Reed, S. Wagner, J.F. Ranville, T. Hofmann, Release of TiO_2 nanoparticles from sunscreens into surface waters: a one-year survey at the old danube recreational lake, Environ. Sci. Technol. 48 (2014) 5415–5422.
[13] M. Bouby, H. Geckeis, F.W. Geyer, Application of asymmetric flow field-flow fractionation (AsFlFFF) coupled to inductively coupled plasma mass spectrometry (ICPMS) to the quantitative characterization of natural colloids and synthetic nanoparticles, Anal. Bioanal. Chem. 392 (2008) 1447–1457.
[14] C. Degueldre, P.Y. Favarger, Colloid analysis by single particle inductively coupled plasma-mass spectroscopy: a feasibility study, Colloids Surf., A 217 (2003) 137–142.
[15] F. Laborda, J. Jimenez-Lamana, E. Bolea, J.R. Castillo, Critical considerations for the determination of nanoparticle number concentrations, size and number size distributions by single particle ICP-MS, J. Anal. At. Spectrom. 28 (2013) 1220–1232.
[16] H.E. Pace, N.J. Rogers, C. Jarolimek, V.A. Coleman, C.P. Higgins, J.F. Ranville, Determining transport efficiency for the purpose of counting and sizing nanoparticles via single particle inductively coupled plasma mass spectrometry, Anal. Chem. 83 (2011) 9361–9369.
[17] K.A. Huynh, E. Siska, E. Heithmar, S. Tadjiki, S.A. Pergantis, Detection and quantification of silver nanoparticles at environmentally relevant concentrations using asymmetric flow field–flow fractionation online with single particle inductively coupled plasma mass spectrometry, Anal. Chem. 88 (2016) 4909–4916.
[18] B. Hetzer, A. Burcza, V. Gräf, E. Walz, R. Greiner, Online-coupling of AF4 and single particle-ICP-MS as an analytical approach for the selective detection of nanosilver release from model food packaging films into food simulants, Food Control (2017) 113–124 2017 v.80.
[19] M. Baalousha, J.R. Lead, Rationalizing nanomaterial sizes measured by atomic force microscopy, flow field-flow fractionation, and dynamic light scattering: sample preparation, polydispersity, and particle structure, Environ. Sci. Technol. 46 (2012) 6134–6142.
[20] M. Hadioui, C. Peyrot, K.J. Wilkinson, Improvements to single particle ICPMS by the online coupling of ion exchange resins, Anal. Chem. 86 (2014) 4668–4674.
[21] W.-.C. Lee, B.-.T. Lee, S. Lee, Y.S. Hwang, E. Jo, I.-.C. Eom, S.-.W. Lee, S.-.O. Kim, Optimisation, evaluation and application of asymmetrical flow field-flow fractionation with single particle inductively coupled plasma mass spectrometry (SP-ICP-MS) to characterise silver nanoparticles in environmental media, Microchem. J. 129 (2016) 219–230.
[22] K. Loeschner, J. Navratilova, R. Grombe, T.P.J. Linsinger, C. Købler, K. Mølhave, E.H. Larsen, In-house validation of a method for determination of silver nanoparticles in chicken meat based on asymmetric flow field-flow fractionation and inductively coupled plasma mass spectrometric detection, Food Chem. 181 (2015) 78–84.
[23] K. Loeschner, J. Navratilova, C. Købler, K. Mølhave, S. Wagner, F. Kammer, E. Larsen, Detection and characterization of silver nanoparticles in chicken meat by asymmetric flow field flow fractionation with detection by conventional or single particle ICP-MS, Anal. Bioanal. Chem. 405 (2013) 8185–8195.
[24] T.M. Nguyen, J. Liu, V.A. Hackley, Fractionation and characterization of high aspect ratio gold nanorods using asymmetric-flow field flow fractionation and single particle inductively coupled plasma mass spectrometry, Chromatography 2 (2015) 422.
[25] A. Barber, S. Kly, M.G. Moffitt, L. Rand, J.F. Ranville, Coupling single particle ICP-MS with field-flow fractionation for characterizing metal nanoparticles contained in nanoplastic colloids, Environ. Sci.: Nano 7 (2020) 514–524.
[26] M.D. Montano, H.R. Badiei, S. Bazargan, J. Ranville, Improvements in the detection and characterization of engineered nanoparticles using spICP-MS with microsecond dwell times, Environ. Sci.: Nano (2014).
[27] O. Borovinskaya, M. Aghaei, L. Flamigni, B. Hattendorf, M. Tanner, A. Bogaerts, D. Gunther, Diffusion- and velocity-driven spatial separation of analytes from single droplets entering an ICP off-axis, J. Anal. At. Spectrom. 29 (2014) 262–271.
[28] S. Naasz, S. Weigel, O. Borovinskaya, A. Serva, C. Cascio, A.K. Undas, F.C. Simeone, H.J.P. Marvin, R.J.B. Peters, Multi-element analysis of single nanoparticles by ICP-MS using quadrupole and time-of-flight technologies, J. Anal. At. Spectrom. 33 (2018) 835–845.
[29] A. Hegetschweiler, O. Borovinskaya, T. Staudt, T. Kraus, Single-Particle Mass Spectrometry of Titanium and Niobium Carbonitride Precipitates in Steels, Anal. Chem. 91 (2019) 943–950.

[30] A. Gondikas, F. von der Kammer, R. Kaegi, O. Borovinskaya, E. Neubauer, J. Navratilova, A. Praetorius, G. Cornelis, T. Hofmann, Where is the nano? Analytical approaches for the detection and quantification of TiO2 engineered nanoparticles in surface waters, Environmental Science: Nano 5 (2018) 313–326.
[31] L. Hendriks, A. Gundlach-Graham, D. Günther, Analysis of Inorganic Nanoparticles by Single-particle Inductively Coupled Plasma Time-of-Flight Mass Spectrometry, CHIMIA Int. J. Chem. 72 (2018) 221–226.
[32] F. Loosli, Z. Yi, J. Wang, M. Baalousha, Improved extraction efficiency of natural nanomaterials in soils to facilitate their characterization using a multimethod approach, Sci. Total Environ. 677 (2019) 34–46.
[33] L. Hendriks, A. Gundlach-Graham, B. Hattendorf, D. Günther, Characterization of a new ICP-TOFMS instrument with continuous and discrete introduction of solutions, J. Anal. At. Spectrom. 32 (2017) 548–561.
[34] M. Tanner, Shorter signals for improved signal to noise ratio, the influence of Poisson distribution, J. Anal. At. Spectrom. 25 (2010) 405–407.
[35] P.J. Wyatt, Measurement of special nanoparticle structures by light scattering, Anal. Chem. 86 (2014) 7171–7183.
[36] G.R. Deen, J.S. Pedersen, Investigation on the structure of temperature-responsive N-isopropylacrylamide microgels containing a new hydrophobic crosslinker, Cogent Chem. 1 (2015) 1012658.
[37] M. Baalousha, M. Sikder, A. Prasad, J. Lead, R. Merrifield, G.T. Chandler, The concentration-dependent behaviour of nanoparticles, Environ. Chem. 13 (2016) 1–3.
[38] M. Baalousha, Aggregation and disaggregation of iron oxide nanoparticles: influence of particle concentration, pH and natural organic matter, Sci. Total Environ. 407 (2009) 2093–2101.
[39] S.M. Rodrigues, T. Trindade, A.C. Duarte, E. Pereira, G.F. Koopmans, P.F.A.M. Römkens, A framework to measure the availability of engineered nanoparticles in soils: trends in soil tests and analytical tools, TrAC Trends Anal. Chem. 75 (2016) 129–140.